

Supporting Information

***In Situ* Nitridated Porous Nanosheet Networked $\text{Co}_3\text{O}_4\text{-Co}_4\text{N}$ Heteronanostructure Supported on Hydrophilic Carbon Cloth for Highly Efficient Electrochemical Hydrogen Evolution**

Bin Liu^a, Junye Cheng^a, Hui-Qing Peng^b, , Da Chen^c, Xiao Cui^d, Dong Shen^d, Kui Zhang^e, Tianpeng Jiao^a, Minfei Li^c, Chun-Sing Lee^d, Wenjun Zhang^{a, f*}

^a Center of Super-Diamond and Advanced Films (COSDAF) & Department of Materials Science and Engineering, City University of Hong Kong, Tat Chee Avenue, Kowloon, Hong Kong, China

^b Department of Chemistry, Institute for Advanced Study, Institute of Molecular Functional Materials and Division of Biomedical Engineering, The Hong Kong University of Science & Technology, Clear Water Bay, Kowloon, Hong Kong, China

^c Department of Mechanical and Biomedical Engineering, City University of Hong Kong, Tat Chee Avenue, Kowloon, Hong Kong, China

^d Center of Super-Diamond and Advanced Films (COSDAF) & Department of Chemistry, City University of Hong Kong, Tat Chee Avenue, Kowloon, Hong Kong, China

^e School of Chemistry and Chemical Engineering, Anhui University of Technology, Ma'anshan, Anhui 243032, China

^f City University of Hong Kong Shenzhen Research Institute, Shenzhen 518057, Guangdong, China

* Corresponding author.

E-mail address: apwjzh@cityu.edu.hk

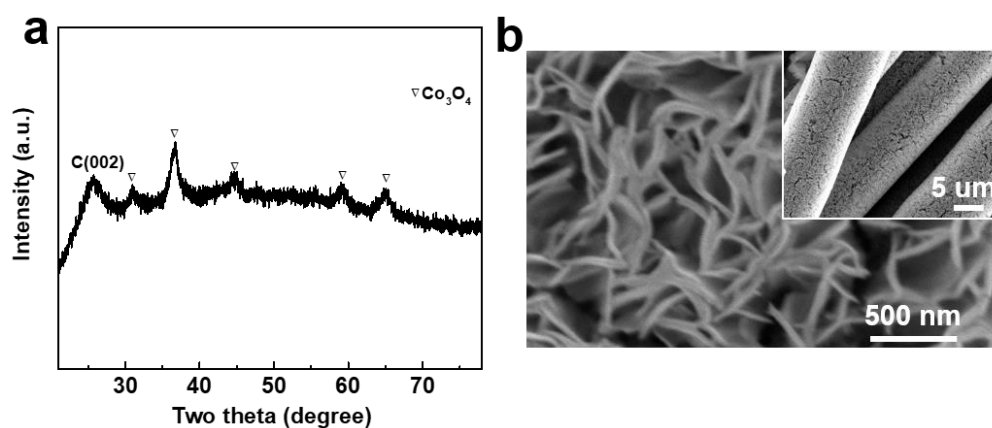


Fig. S1. (a) XRD pattern and (b) SEM images of $\text{Co}_3\text{O}_4/\text{HCC}$ obtained by heat treatment of as-prepared $\alpha\text{-Co}(\text{OH})_2/\text{HCC}$ at $300\text{ }^\circ\text{C}$ for 1 h under air atmosphere. The Co_3O_4 nanosheets formed apparently an interconnected network structure.

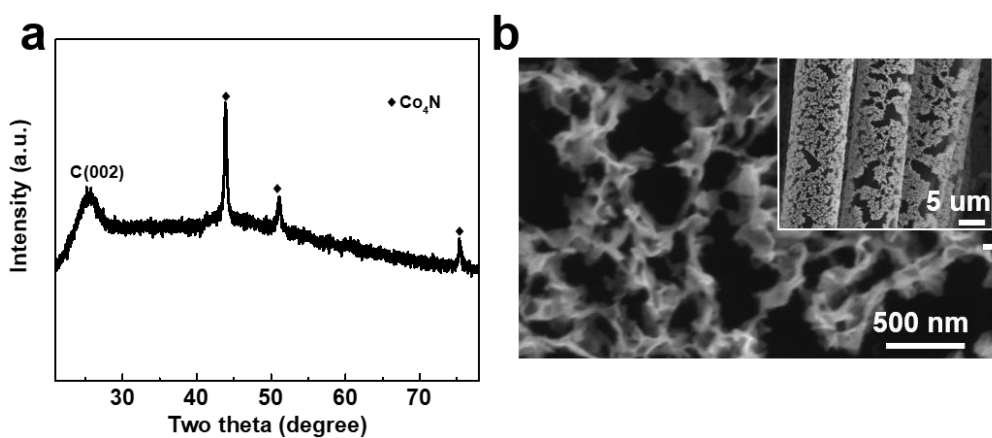


Fig. S2. (a) XRD pattern and (b) SEM images of $\text{Co}_4\text{N}/\text{HCC}$ obtained by heat treatment of as-prepared $\alpha\text{-Co}(\text{OH})_2/\text{HCC}$ at $400\text{ }^\circ\text{C}$ for 1 h under NH_3 atmosphere. The Co_4N nanosheets also formed a networked structure.

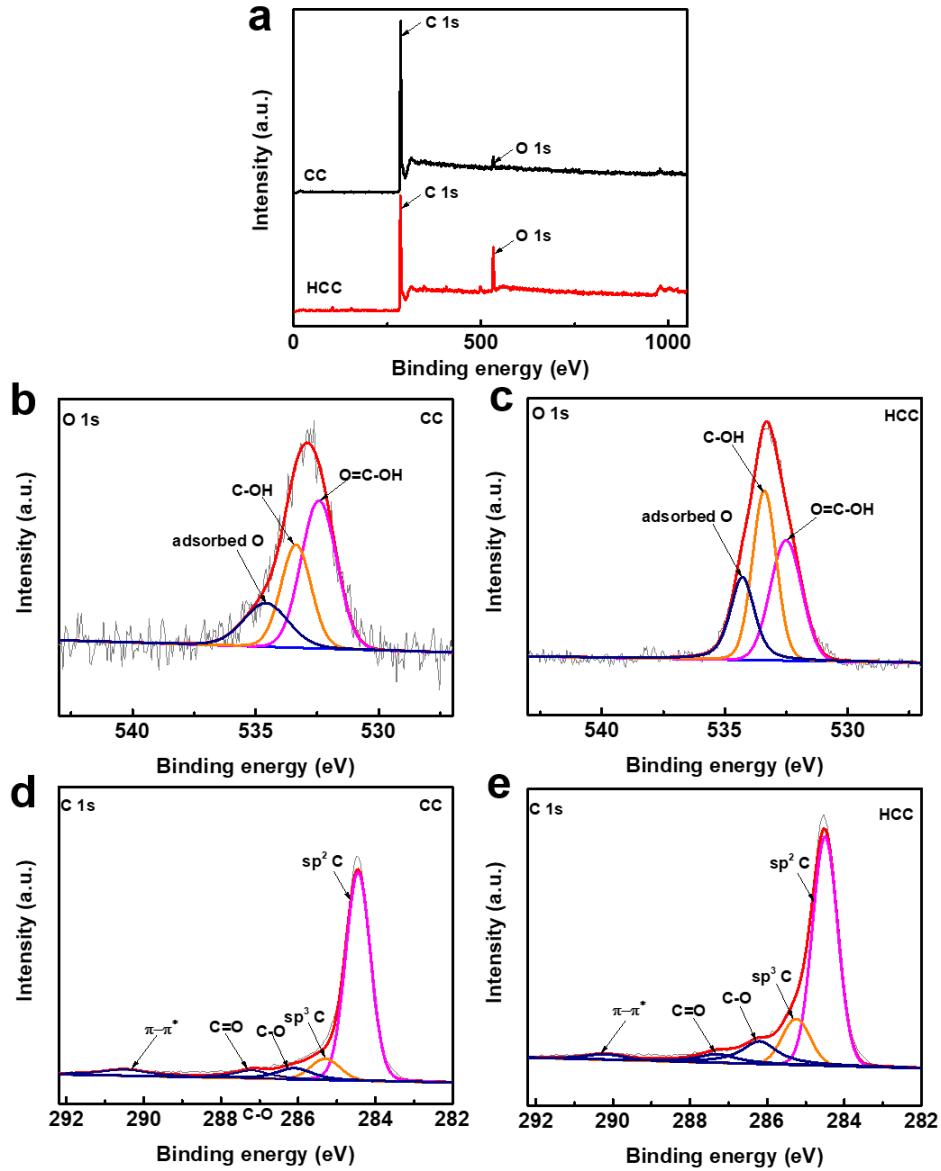


Fig. S3. (a) XPS survey spectra of CC and HCC. High-resolution spectra of O 1s (b) CC and (c) HCC, and high-resolution C 1s spectra of (d) CC and (e) HCC.

The C 1s peak in the XPS spectra can be split into five peaks at 284.5, 285.3, 286.1, 287.2, and 290.5 eV, which can be attributed to sp^2 -bonded carbon, sp^3 -bonded carbon, C-O groups, C=O groups, and $\pi-\pi^*$ shake-up satellites, respectively.¹ The O 1s peak can be deconvoluted into three components, i.e., the peak at 532.4 eV for the carboxyl group (COO^-), the peak at 533.3 eV for the hydroxyl (C-OH), and the peak at 534.6 eV for the chemisorbed oxygen.^{2, 3} The content of C-OH and adsorbed oxygen increase after hydrogen plasma treatment. The increase in oxygen content can be attributed to edge-dangling bonds induced by the plasma treatment, which can either bind with oxygen to form oxygen-containing functional groups (e.g., C-OH) or adsorb water or oxygen when exposed to air.

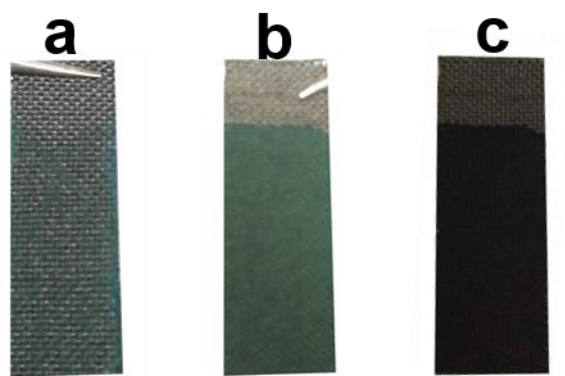


Fig. S4. Optical images of (a) $\alpha\text{-Co(OH)}_2$ nanosheets grown on the untreated CC, (b) $\alpha\text{-Co(OH)}_2$ nanosheets grown on HCC, and (c) $\text{Co}_3\text{O}_4\text{-Co}_4\text{N}$ porous nanosheet networks grown on HCC.

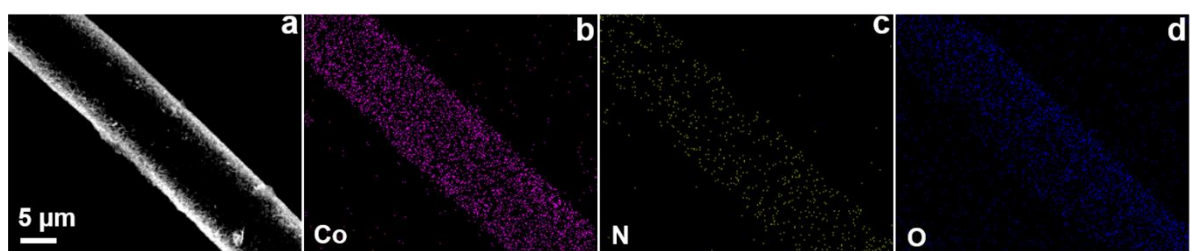


Fig. S5. SEM image and the corresponding elements mapping of $\text{Co}_3\text{O}_4\text{-Co}_4\text{N}/\text{HCC}$ showing the distribution of (b) Co, (c) N, and (d) O over the surface of carbon fiber.

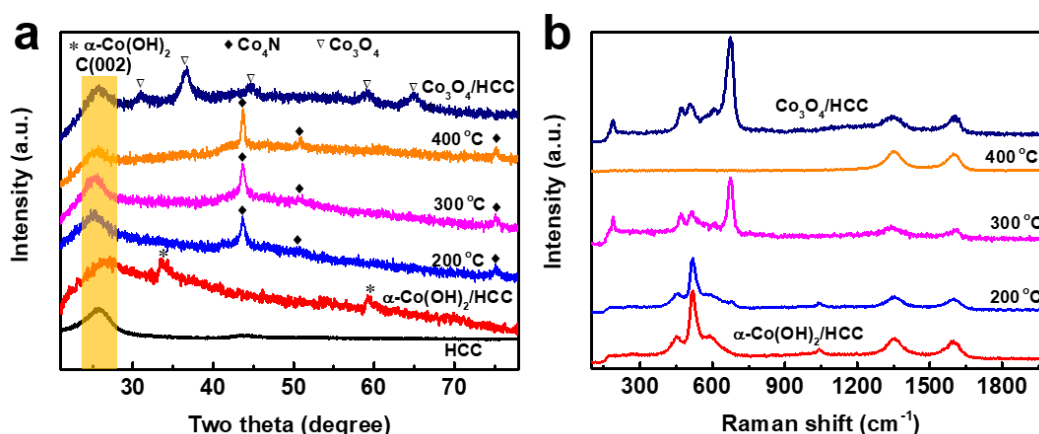


Fig. S6. (a) XRD patterns of HCC, $\alpha\text{-Co(OH)}_2/\text{HCC}$, $\text{Co}_3\text{O}_4/\text{HCC}$, and the obtained products after nitrogen plasma treatment of $\alpha\text{-Co(OH)}_2/\text{HCC}$ at different temperatures. (b) The corresponding Raman spectra of the samples.

XRD patterns showed that all the products after nitrogen plasma treatment at 200 °C, 300 °C and 400 °C contained Co_4N phase. However, due to the poor sensitivity of Raman spectroscopy to Co_4N ,⁴ the Raman spectra of the corresponding samples only revealed $\alpha\text{-Co(OH)}_2$ signal for the sample obtained at 200 °C, and Co_3O_4 signal for the sample obtained at 300 °C. For the sample obtained at 400 °C, no additional bands besides the characteristic D ($\sim 1350\text{ cm}^{-1}$) and G ($\sim 1600\text{ cm}^{-1}$) peaks of HCC substrate were observed. The combination of the XRD and Raman results suggested that the $\alpha\text{-Co(OH)}_2$ was partially nitridated to Co_4N at 200 °C, and the decomposition and nitridation of $\alpha\text{-Co(OH)}_2$ occurred simultaneously at an elevated temperature of 300 °C, leading to the formation of $\text{Co}_4\text{N}\text{-Co}_3\text{O}_4$ hybrid. When the temperature was increased to 400 °C, only Co_4N phase was obtained.

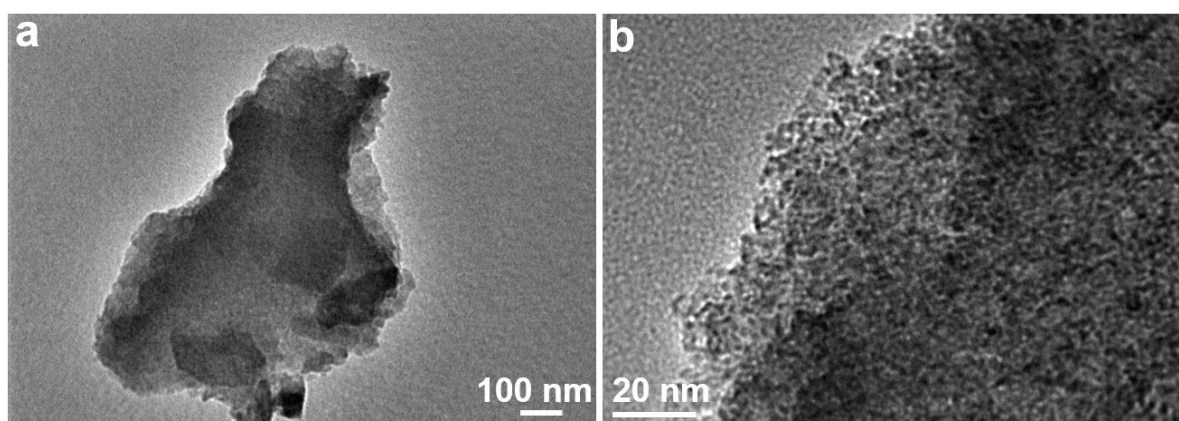


Fig. S7. TEM images of $\alpha\text{-Co(OH)}_2$ nanosheets.

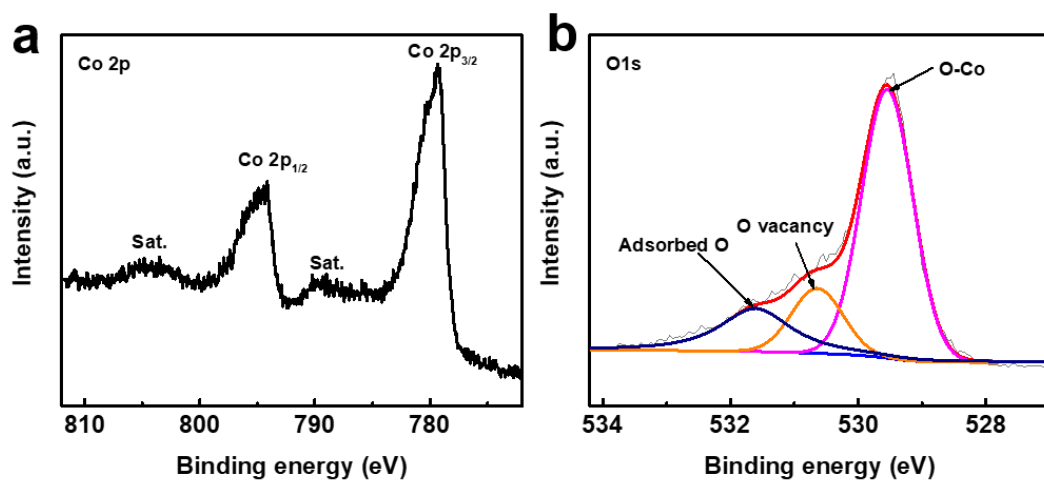


Fig. S8. High-resolution XPS spectra of (a) Co 2p and (b) O 1s of Co_3O_4 .

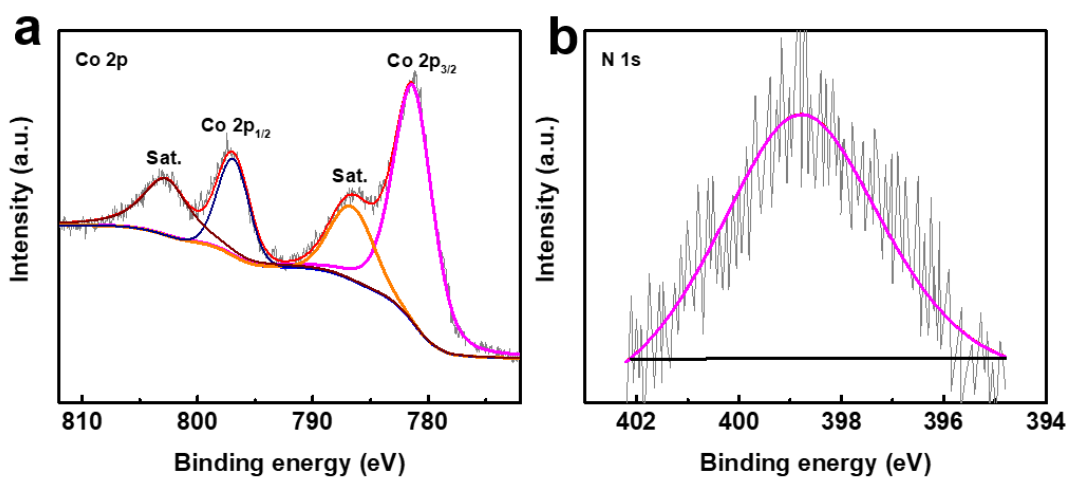


Fig. S9. High-resolution XPS spectra of (a) Co 2p and (b) N 1s of Co_4N .

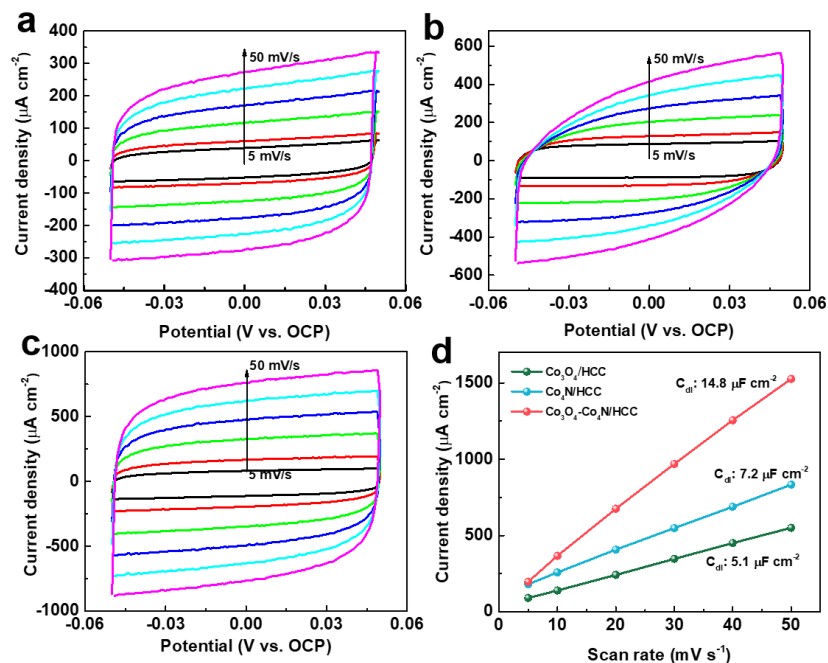


Fig. S10. (a) The CV curves of samples measured at different scan rates of 5, 10, 20, 30, 40, and 50 mV s^{-1} in CH_3CN with 0.15 M KPF_6 . (a) $\text{Co}_3\text{O}_4/\text{HCC}$, (b) $\text{Co}_4\text{N}/\text{HCC}$, and (c) $\text{Co}_3\text{O}_4\text{-Co}_4\text{N}/\text{HCC}$. (d) The dependence of difference between the anodic and cathodic current densities at the open circuit potential (OCP) on the scan rate of potential obtained on $\text{Co}_3\text{O}_4/\text{HCC}$, $\text{Co}_4\text{N}/\text{HCC}$ and $\text{Co}_3\text{O}_4\text{-Co}_4\text{N}/\text{HCC}$.

The double layer capacitance (C_{dl}) was calculated through the slope of linear dependences divided by 2,⁵ which could be considered as an indication of the electrochemically active surface areas of the samples.

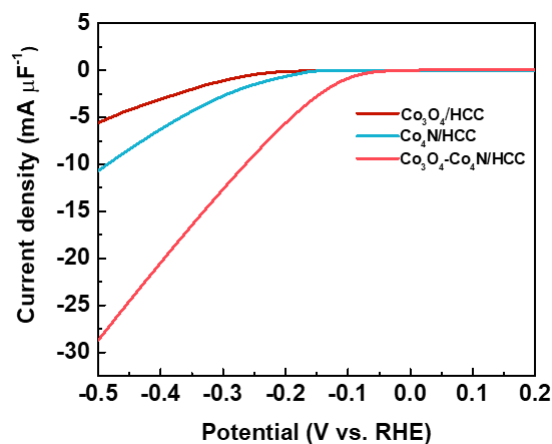


Fig. S11. Polarization curves normalized by the electrochemical double-layer capacitances of $\text{Co}_3\text{O}_4/\text{HCC}$, $\text{Co}_4\text{N}/\text{HCC}$, and $\text{Co}_3\text{O}_4\text{-Co}_4\text{N}/\text{HCC}$.

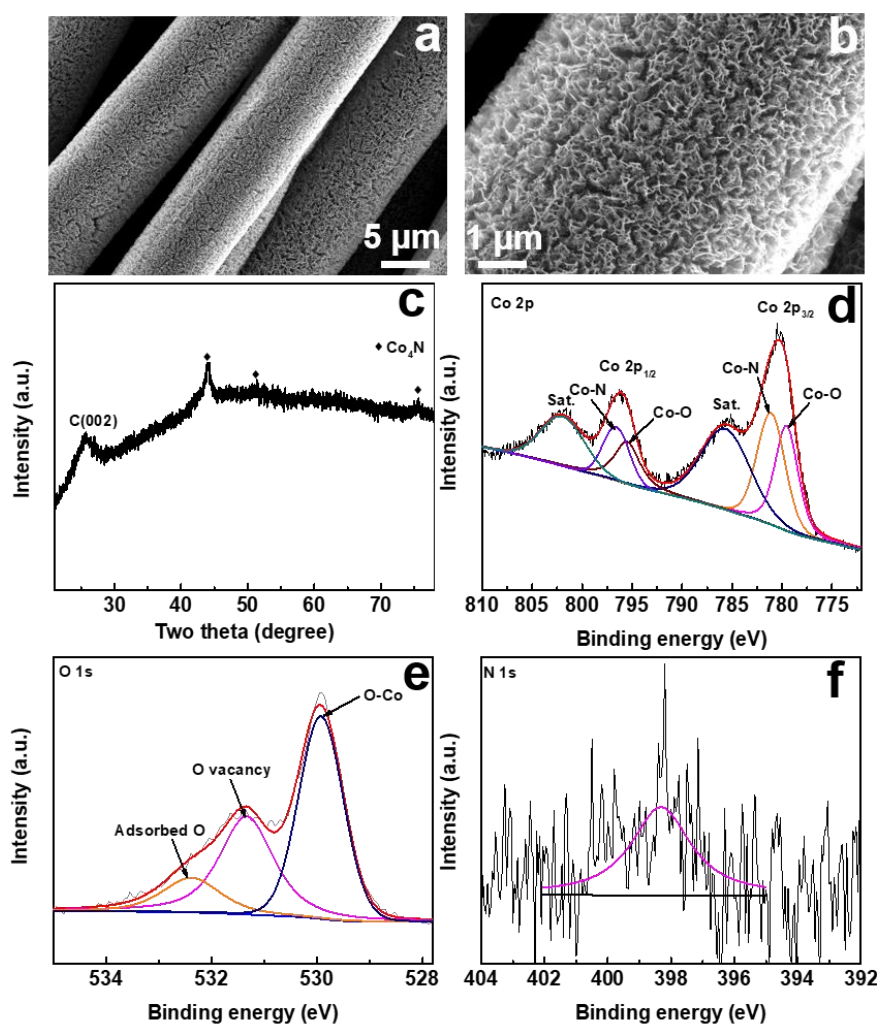


Fig. S12. (a, b) The SEM surface images and (c) XRD pattern of the $\text{Co}_3\text{O}_4\text{-Co}_4\text{N}/\text{HCC}$ after HER stability measurement for 40 h in 1.0 M KOH solution. The corresponding high-resolution XPS spectra of (d) Co 2p, (e) O 1s and (f) N 1s of the sample.

Table S1. The C and O contents of CC and HCC from XPS measurement.

Sample	C percent(%)	O percent (%)	O/C ratio
CC	96.92	3.08	0.032
HCC	87.78	12.22	0.139

Table S2. EDX analysis on the elemental compositions of the samples prepared by nitrogen plasma treatment with different durations.

Samples	Atomic percentage (%)		
	Co	O	N
5 min	55.7	41.2	3.1
10 min	63.7	30.7	5.6
15min	70.2	21.3	8.5
20 min	74.0	15.4	10.6

Table S3. Comparison of the HER activity of the with other non-noble metal-based electrocatalysts with decent performance in basic condition.

Catalysts	Electrolyte	Current density (mA cm ⁻²)	Overpotential (mV)	Tafel slope (mV dec ⁻¹)	Reference
Co ₃ O ₄ -Co ₄ N/HCC	1.0 M KOH	10	90	57.8	This work
Co-MoS ₂ /CC	1.0 M KOH	10	203	158	<i>Energy Environ. Sci.</i> 2016 , 9, 2789.
Ni-P/carbon paper	1.0 M KOH	10	100	85.4	<i>Adv. Funct. Mater.</i> 2016 , 26, 4067.
Fe-CoP/Ti	1.0 M KOH	10	78	75	<i>Adv. Mater.</i> 2017 , 29, 1602441.
Ni-MoS ₂ /CC	1.0 M KOH	10	98	60	<i>Energy Environ. Sci.</i> 2016 , 9, 2789.
MoC _x nano-octahedrons	1.0 M KOH	10	151	59	<i>Nat. Commun.</i> 2015 , 6, 6512.
MoS ₂ /NiCo-LDH/CFP	1.0 M KOH	10	78	77	<i>Joule</i> , 2017 , 1, 383.
Co-Ni ₃ N nanorods	1.0 M KOH	10	194	156	<i>Adv. Mater.</i> 2018 , 30, 1705516.
CoP nanowires	1.0 M KOH	10	209	129	<i>J. Am. Chem. Soc.</i> 2014 , 136, 7587.
NiCo ₂ S ₄ nanowire/NF	1.0 M KOH	10	210	58.9	<i>Adv. Funct. Mater.</i> 2016 , 26, 4661.
Ni-NiO/N-rGO	1.0 M KOH	10	135	46	<i>Adv. Funct. Mater.</i> 2015 , 25, 5799.
Ni ₂ P/Fe ₂ P	1.0 M KOH	10	121	67	<i>Adv. Energy Mater.</i> 2018 , 8, 1800484.
Se-(NiCo)S _x /(OH) _x	1.0 M KOH	10	103	87.3	<i>Adv. Mater.</i> 2018 , 30, 1705538.
Co/CoP	1.0 M KOH	10	253	73.8	<i>Adv. Energy Mater.</i> 2017 , 7, 1602355.
Mn-Co-P	1.0 M KOH	10	76	52	<i>ACS Catal.</i> 2016 , 7, 98.
Ni ₅ P ₄ /Ni foil	1.0 M KOH	10	150	53	<i>Angew. Chem. Int. Ed.</i> 2015 , 127, 12538.

Ni _{0.89} Co _{0.11} Se ₂ MNSN/NF	1.0 M KOH	10	85	52	<i>Adv. Mater.</i> 2017 , 29, 1606521.
NiMoN/CC	1.0 M KOH	10	109	95	<i>Adv. Energy Mater.</i> 2016 , 6, 1600221.
N-Ni ₃ S ₂ /NF	1.0 M KOH	10	110	-	<i>Adv. Mater.</i> 2017 , 29, 1701584.
V-Co ₄ N nanosheets	1.0 M KOH	10	37	44	<i>Angew. Chem. Int. Ed.</i> 2018 , 130, 5170.
3D Ni–Mo alloy	1.0 M NaOH	20	34	-	<i>ChemElectroChem</i> 2014 , 1, 1138.
Co–Mo–P	1.0 M KOH	10	30 ~ 35	63	<i>ChemCatChem</i> 2018 , 10, 4832.
MoNi ₄ /MoO ₂ @Ni	1.0 M KOH	10	15	30	<i>Nat. Commun.</i> 2017 , 8, 15437.

Table S4. The overpotential at the current density of 10 mA cm⁻² (η_{10}), Tafel slope, MA, TOF, C_{dl} , and R_{ct} of the samples from electrocatalytic HER tests.

Catalysts	η_{10} (mV)	Tafel slope (mV dec ⁻¹)	MA (A g ⁻¹)	TOF (s ⁻¹)	C_{dl} (μ F cm ⁻²)	R_{ct} (Ω)
Co ₃ O ₄ -Co ₄ N/HCC	90	57.8	50.6	0.02	14.8	6
Co ₄ N/HCC	245	87.9	4.05	0.0016	7.2	16
Co ₃ O ₄ /HCC	348	136.7	0.95	0.00038	5.1	144

References

1. L. Tao, Q. Wang, S. Dou, Z. Ma, J. Huo, S. Wang and L. Dai, *Chem. Commun.*, 2016, **52**, 2764-2767.
2. L.-Z. Fan, S. Qiao, W. Song, M. Wu, X. He and X. Qu, *Electrochim. Acta* 2013, **105**, 299-304.
3. I.-Y. Jeon, H.-J. Choi, S.-M. Jung, J.-M. Seo, M.-J. Kim, L. Dai and J.-B. Baek, *J. Am. Chem. Soc.*, 2012, **135**, 1386-1393.
4. G. Gubert, E. Ribeiro, J. Varalda, A. G. Bezerra, W. H. Schreiner and D. H. Mosca, *J. Alloys Compd.*, 2017, **725**, 519-525.
5. Y. Yoon, B. Yan and Y. Surendranath, *J. Am. Chem. Soc.*, 2018, **140**, 2397-2400.